Two-Dimensional Computational Model of Energy Gain in NIF Capsules

K. ANDERSON, R. BETTI and T. A. Gardiner

University of Rochester
Laboratory for Laser Energetics

Abstract

A two-dimensional hydrodynamic code is employed to describe the implosion of a NIF-like ICF capsule beginning from the free-fall phase to determine its energy gain. Data are taken from one-dimensional code *LILAC* at the end of the acceleration phase, and single- or multimode perturbations are then introduced in the inner shell surface. The data are then input into a two-dimensional hydrodynamic code employing a uniformly moving mesh, the motion of which is determined by the trajectory of the capsule shell. Energy gain is then analyzed as a function of the pertubation amplitude for single-mode perturbations or of the mean-square perturbation amplitude for multimode perturbations. Alpha-particle energy deposition is treated diffusively in this model using a single energy group for faster computation.

A fast 2-D moving-grid eulerian code has been developed to simulate deceleration phase, ignition, and burn of ICF capsules

- The code includes the essential physics: two fluids, thermal transport, and one-group alpha diffusion. The goal is to compile a large database of various runs to correlate the effects of the Rayleigh–Taylor instability on fusion energy yield.
- The full multimode simulation of the deceleration, ignition, and burn on a 300×300 grid may be run in about an hour on a fast PC.
- As input, we use output from the 1-D code *LILAC* at the end of the acceleration phase. Multimode velocity perturbations are introduced to simulate expected 2-D distortion.

The model is based on an operator-splitting technique between hydrodynamics and transport. It includes single mass and momentum equations, while solving a separate energy equation for electrons and ions

- We use a single-fluid model, including an additional energy conservation equation, to calculate the electron pressure:

Mass conservation
$$\frac{\partial \rho}{\partial \mathbf{t}} + \nabla \bullet (\rho \mathbf{v}) = \mathbf{0}$$

Momentum conservation
$$\rho\left(\frac{\partial \mathbf{v}}{\partial \mathbf{t}} + \mathbf{v} \bullet \nabla \mathbf{v}\right) = -\nabla \mathbf{P}$$

Total energy conservation
$$\frac{\partial}{\partial \mathbf{t}}\left[\rho\left(\mathbf{e} + \frac{\mathbf{1}}{\mathbf{2}}\nu^{\mathbf{2}}\right)\right] + \nabla \bullet \left\{\mathbf{v}\left[\rho\left(\mathbf{e} + \frac{\mathbf{1}}{\mathbf{2}}\nu^{\mathbf{2}}\right) + \mathbf{P}\right]\right\} = \mathbf{0}$$

- We use the ideal gas equation of state:

$$\mathbf{P} = \frac{\rho \mathbf{T}(\mathbf{1} + \mathbf{Z})}{\mathbf{m_i}}$$

- A simple manipulation of the electron energy equation leads to the following conservative form:

$$\frac{\partial \mathbf{P_e^{3/5}}}{\partial \mathbf{t}} + \nabla \bullet \left(\mathbf{v}\mathbf{P_e^{3/5}}\right) = \mathbf{0}$$

The code makes use of a cylindrical grid

- We choose to solve the hydrodynamic equations in cylindrical coordinates, assuming no variation in φ.
- This avoids small grid spacing in θ for small *r*, thereby allowing a larger timestep.

$$\frac{\partial}{\partial t}(r\rho) + \frac{\partial}{\partial r}(r\rho v_r) + \frac{\partial}{\partial z}(r\rho v_z) = 0$$

$$\frac{\partial}{\partial t}(r\rho v_r) + \frac{\partial}{\partial r}\left[r\left(\rho v_r^2 + P\right)\right] + \frac{\partial}{\partial z}(r\rho v_r v_z) + P = 0$$

$$\frac{\partial}{\partial t}(r\rho v_z) + \frac{\partial}{\partial r}(r\rho v_r v_z) + \frac{\partial}{\partial z}\left[r\left(\rho v_z^2 + P\right)\right] = 0$$

$$\frac{\partial}{\partial t}\left[r\left(\frac{P}{\gamma - 1} + \frac{1}{2}\rho v^2\right)\right] + \frac{\partial}{\partial r}\left[r\, v_r\left(\frac{\gamma P}{\gamma - 1} + \frac{1}{2}\rho v^2\right)\right] + \frac{\partial}{\partial z}\left[r v_z\left(\frac{\gamma P}{\gamma - 1} + \frac{1}{2}\rho v^2\right)\right] = 0$$

$$\frac{\partial}{\partial t}\left(rP_e^{3/5}\right) + \frac{\partial}{\partial r}\left(r v_r P_e^{3/5}\right) + \frac{\partial}{\partial z}\left(r v_z P_e^{3/5}\right) = 0$$

A uniformly compressing Eulerian grid allows for higher resolution near stagnation

- **Moving-grid variable transformation:** $\xi = \dfrac{r}{R(t)}, \eta = \dfrac{z}{R(t)}$
- **This yields the following set of equations:** $\dfrac{\partial U}{\partial t} + \dfrac{\partial F}{\partial \xi} + \dfrac{\partial G}{\partial \eta} + H = 0,$

$$U = \begin{bmatrix} \rho\xi R^3 \\ \xi R^3 \rho \nu_r \\ \xi R^3 \rho \nu_z \\ \xi R^3 \left(\dfrac{P}{\gamma - 1} + \dfrac{1}{2}\rho\nu^2 \right) \\ P_e^{3/5} \xi R^3 \end{bmatrix} \qquad F = \begin{bmatrix} \rho\xi R^2 \left(\nu_r - \xi\dot{R}\right) \\ \xi R^2 \left[\rho\nu_r \left(\nu_r - \xi\dot{R}\right) + P\right] \\ R^2 \rho\nu_z \left(\nu_r - \xi\dot{R}\right) \\ R\left\{ \xi R^3 \left(\nu_r - \xi\dot{R}\right)\left(\dfrac{P}{\gamma - 1} + \dfrac{1}{2}\rho\nu^2\right) + \xi R \nu_r P \right\} \\ P_e^{3/5}\xi R^2 \left(\nu_r - \xi\dot{R}\right) \end{bmatrix}$$

$$G = \begin{bmatrix} \rho\xi R^2 \left(\nu_z - \eta\dot{R}\right) \\ \xi R^2 \rho\nu_r \left(\nu_z - \eta\dot{R}\right) \\ \xi R^2 \left[\rho\nu_z \left(\nu_z - \eta\dot{R}\right) + P\right] \\ R\left\{ \xi R^3 \left(\nu_z - \eta\dot{R}\right)\left(\dfrac{P}{\gamma - 1} + \dfrac{1}{2}\rho\nu^2\right) + \xi R \nu_z P \right\} \\ P_e^{3/5}\xi R^2 \left(\nu_z - \eta\dot{R}\right) \end{bmatrix} \qquad H = \begin{bmatrix} 0 \\ PR^2 \\ 0 \\ 0 \\ 0 \end{bmatrix}$$

The code treats heat conduction diffusively and uses an analytical solution for temperature equilibration

- **Heat conduction equation using Spitzer thermal conductivity:**

$$\rho c_v \frac{\partial T_{e,i}}{\partial t} = \nabla \bullet \kappa_{e,i} \nabla T_{e,i}, \qquad \kappa_{e,i} \propto \sqrt{\frac{m_e}{m_{e,i}}} T_{e,i}^{5/2}$$

- **Analytically solve the equation for ion and electron temperature equilibration at each time step using the electron-ion equilibration time:**

$$\frac{\partial}{\partial t}(P_e - P_i) = \frac{(P_e - P_i)}{\tau_{equil}}$$

with the solution

$$(P_e - P_i) = (P_e - P_i)_0 e^{-dt/\tau_{equil}}$$

Alpha transport is treated with a single-group diffusion model

- **To further shorten computation time, we treat alpha transport using a single diffusion equation for the alpha-particle energy density ε_α:**

$$\frac{\partial \varepsilon_\alpha}{\partial \mathbf{t}} + \mathbf{v} \bullet \nabla \varepsilon_\alpha - \nabla \bullet \mathbf{D} \nabla \varepsilon_\alpha + \frac{\varepsilon_\alpha}{\mathbf{t_{relax}}} = \mathbf{gE_0},$$

$$\mathbf{D} = \left(\mathbf{47}\,\mu\mathbf{m^2/ps}\right) \frac{\mathbf{T_e^{3/2}(keV)}}{\rho\left(\mathbf{g / cm^3}\right)}, \qquad \mathbf{E_0} = \mathbf{3.5\,MeV}$$

$$\mathbf{t_{relax}} = \frac{\mathbf{3\sqrt{2}}}{\mathbf{16}\pi} \frac{\mathbf{m}_\alpha \mathbf{T_e^{3/2}}}{\mathbf{L}_{\alpha/\mathbf{e}}\left(\mathbf{Z}_\alpha \mathbf{e^2}\right)^{\mathbf{2}} \mathbf{n_e m_e^{1/2}}}, \qquad \mathbf{g} = \frac{\rho^{\mathbf{2}}}{\mathbf{4m_i}} \langle \sigma \nu \rangle.$$

Notes on computational methods used

- Algorithms used
  - The hydrodynamics equations are treated using a predictor–corrector, MacCormack, scheme. Also, the electron pressure and alpha-particle energy are convected using the same scheme according to the equation given for electron pressure.
  - The heat conduction and alpha diffusion equations are treated with a Crank–Nicholson diffusion solver.
  - Bremsstrahlung radiation is treated as a sink term in the energy equation.
- Stability of algorithm
  - Due to the strong shocks present in ICF implosions, artificial terms were added to simulate both viscosity and heat conduction to prevent oscillations near shock fronts.

Evolution of shell density, ℓ = 20 (single mode), inner surface velocity perturbation = 20% of implosion velocity

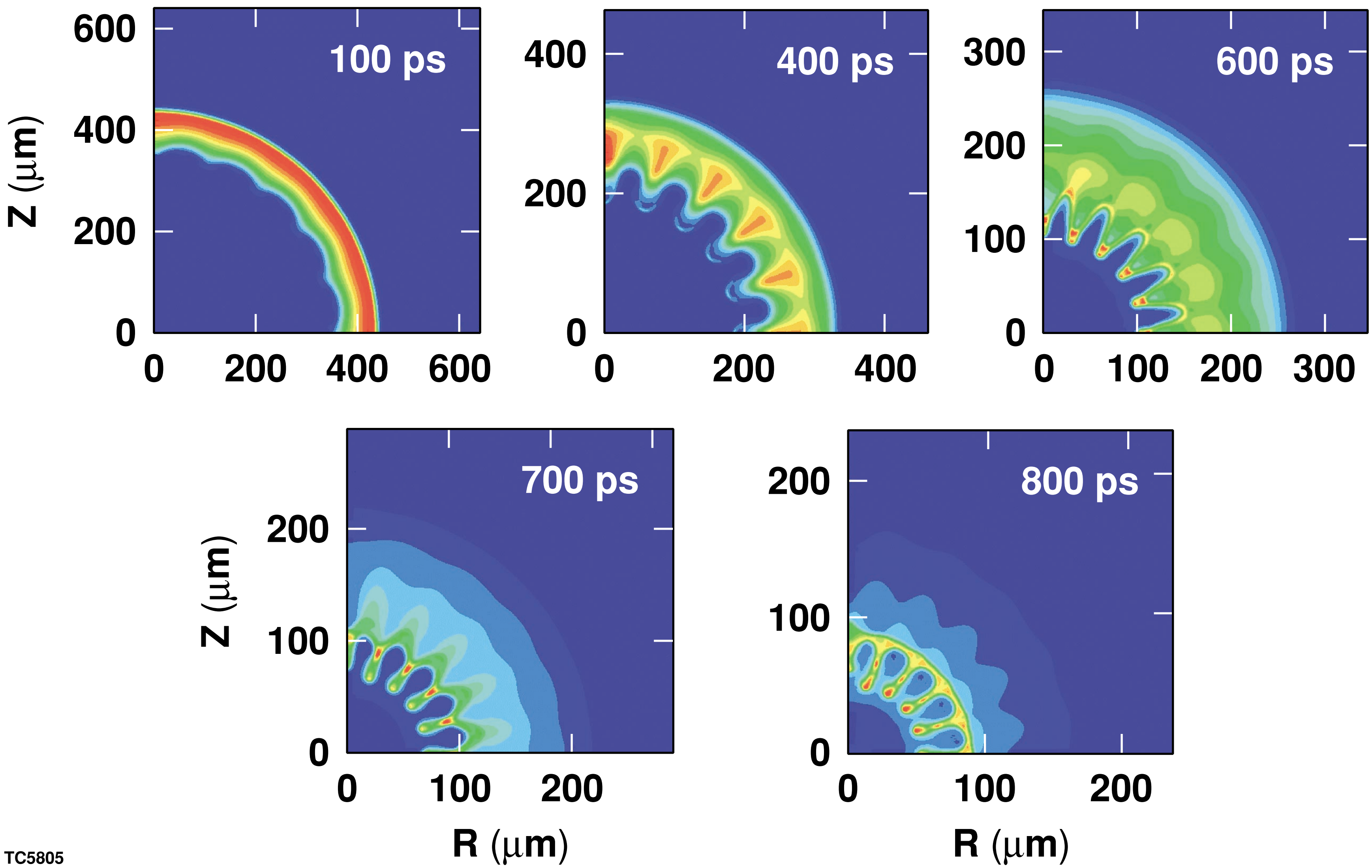

TC5805

Two-dimensional simulations show that the stabilizing effect of hot-spot ablation significantly reduces the deceleration RT growth well into the nonlinear regime

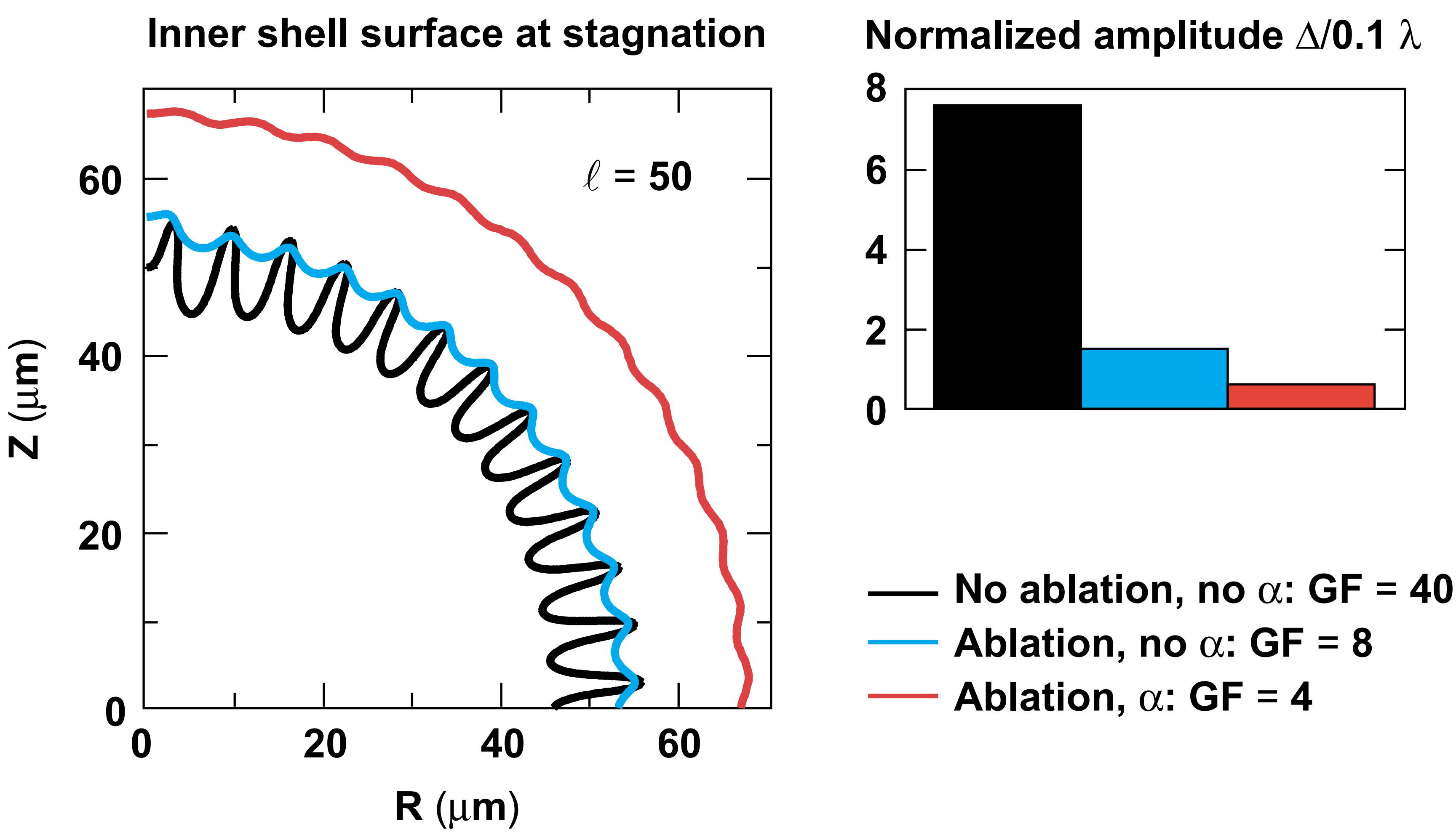

TC5770

The code has been tested for single-mode inner-surface velocity perturbations

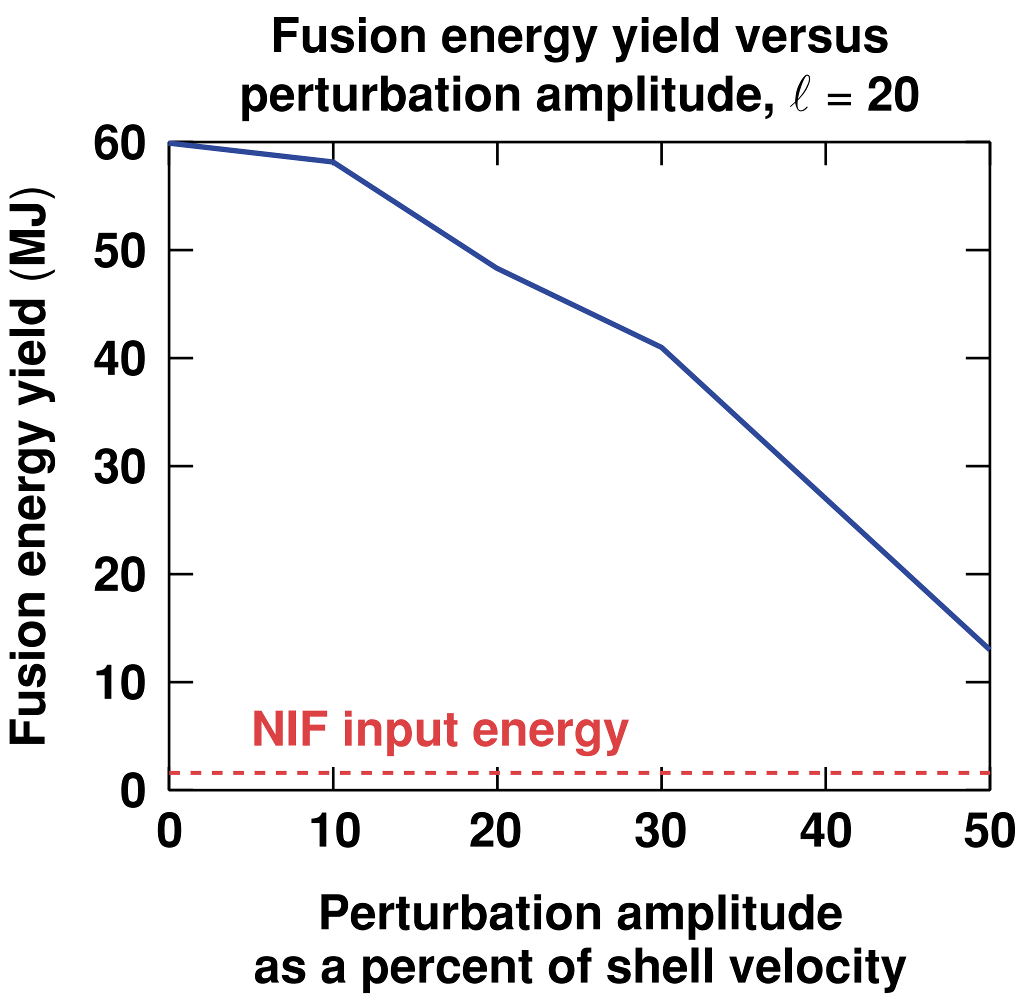

- Output energies for low perturbation amplitude (ℓ = 20) are still significant fractions of the 1-D energy output.
- Other perturbation modes gave higher energy yields, suggesting that ℓ = 20 is probably the most damaging mode.
- Similar graphs for other ℓ modes and for surface perturbations are in progress.

TC5807

Preliminary runs agree qualitativly with predicted models of the deceleration phase of implosion

- Note that for perturbation modes ℓ = 10, ℓ = 30, and ℓ = 40, the energy yield is greater than for the ℓ = 20 mode, given the same initial perturbation amplitude. This is in accordance with the linear theory of the deceleration-phase instability by Betti *et al*. (LLE Review 85).
- From the gain plot for ℓ = 20, one can see that the gain is not significantly affected for pertubation amplitudes of 30% or less. Note that these inner-shell perturbations are centered in a region of the shell, which is relatively low density. Due to this, outer-surface perturbations affect the integrity of the shell more significantly and ultimately fusion energy yield.

A multimode perturbation weighted at low modes breaks the capsule shell, giving low YOC

- A flat-spectrum multimode simulation with $\tilde{\nu} = 0.2\nu_{shell}$ for all even modes ($\ell = 2$ to 40) shows a broken capsule and a small hot spot, giving a yield of 4.8 MJ (YOC = 0.08).

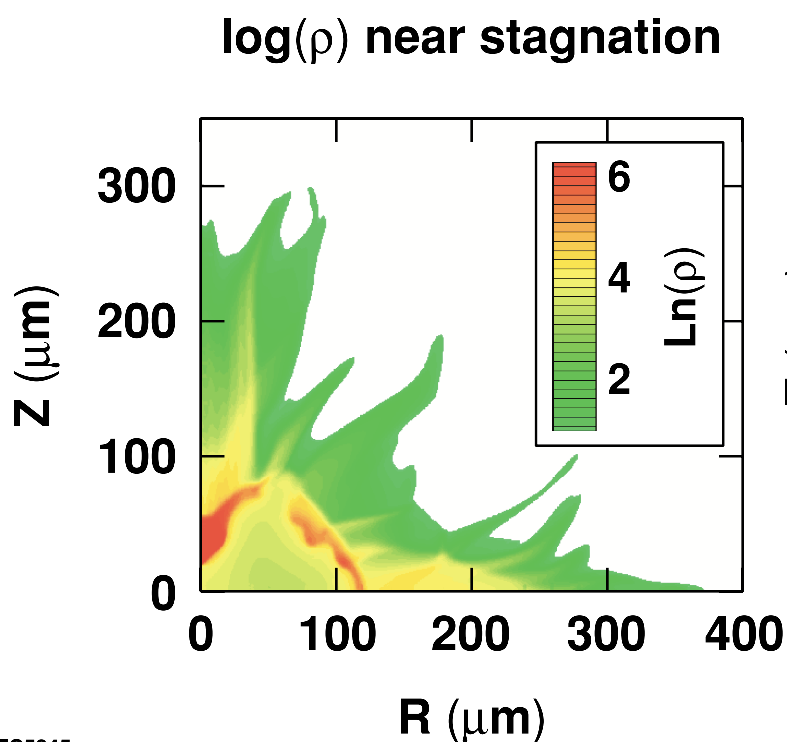

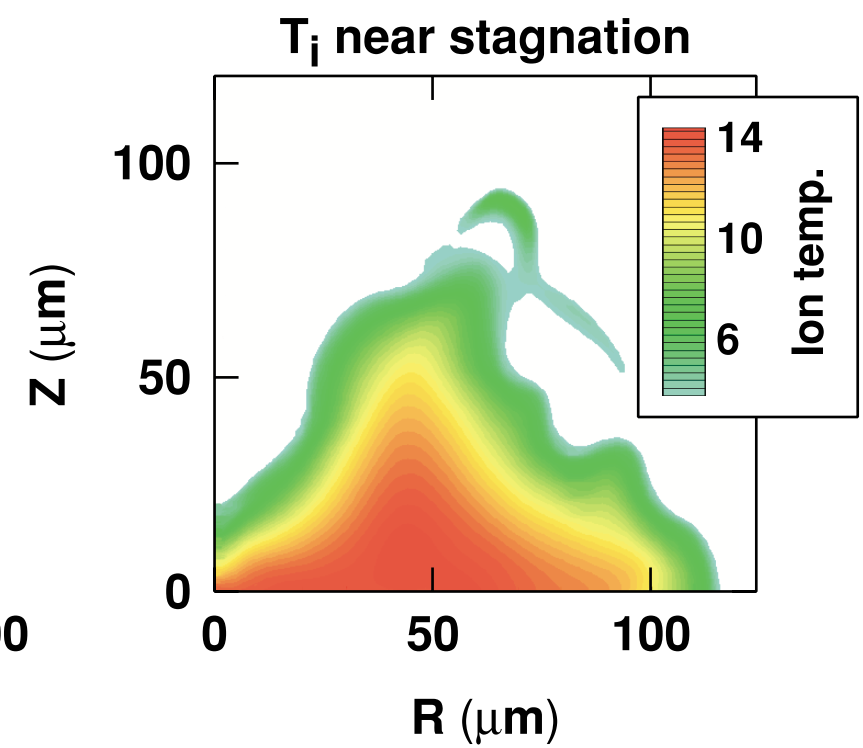

TC5845

2-D simulations with outer-surface nonuniformities show that only low-ℓ modes feed through and grow, causing hot-spot distortion

- Modes ℓ = 2 to 100; velocity perturbation with kinetic energy = 2.7 kJ; linearly decaying spectrum; gain = 47 MJ, YOC = 80%

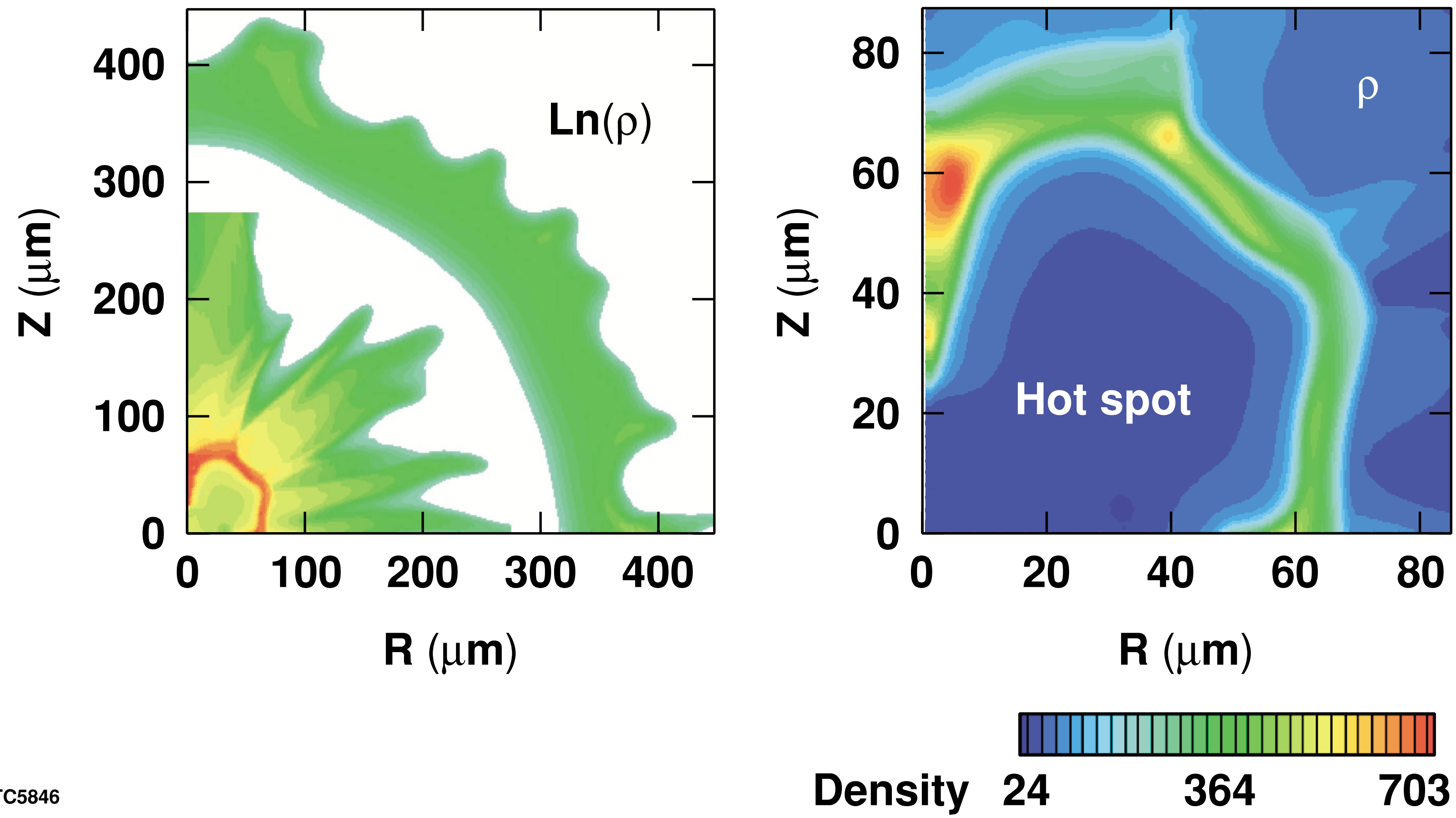

TC5846

The code maintains high resolution at stagnation

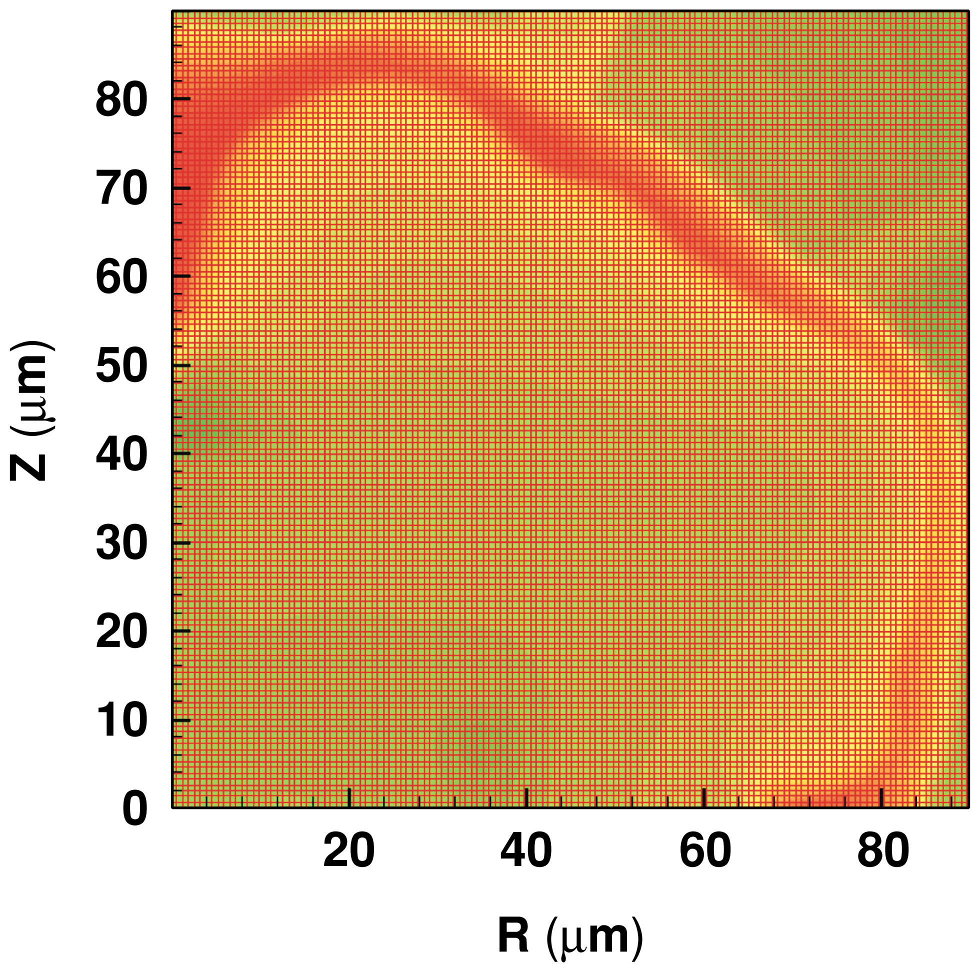

- This plot shows the hot-spot resolution (400×400 total grid size) near stagnation. A log(ρ) plot is superimposed to show the shell size.
- This same simulation took approximately three hours to complete on a PC.

Conclusions

- We have written a fast 2-D code capable of simulating an ICF implosion (from free-fall to ignition and burn wave propagation) on a high-resolution grid (400×400), which runs about three hours on a fast PC.
- Preliminary results of both single- and multimode simulations support existing theories of 2-D Rayleigh–Taylor instability, showing that perturbation modes around $\ell = 20$ most significantly affect the fusion energy yield.

Reference:

R. Betti, M. Umansky, V. Lobatchev, V. N. Goncharov, and R. L. McCrory, LLE Review 85, 1–10 (2001).